Cement and Concrete Composites 127 (2022) 104399

Contents lists available at ScienceDirect

Cement and Concrete Composites

journal homepage: www.elsevier.com/locate/cemconcomp

Durability of high-performance self-compacted concrete using electric arc furnace slag aggregate and cupola slag powder

I. Sosa, C. Thomas *, J.A. Polanco, J. Setién, J.A. Sainz-Aja, P. Tamayo

LADICIM (Laboratory of Materials Science and Engineering), University of Cantabria. E.T.S. de Ingenieros de Caminos, Canales y Puertos, Av./Los Castros 44, 39005, Santander, Spain

ARTICLE INFO

Keywords:
Self-compacting concrete
High-performance concrete
EAFS
Cupola slag
Electric arc furnace slag
Durability
Mechanical properties

ABSTRACT

The current trend in the development of self-compacting concrete with sustainable construction materials has served as a guide to design a novel self-compacting concrete, with siderurgical by-products (steel slag aggregates and cupola slag powder as supplementary cementing material) that also meets the demands of high-performance concrete. This research sets out to clarify the unknown behavior of slag concrete, its durability, which is the ability to withstand any process that tends to deteriorate it. In order to assess the durability of this eco-friendly concrete, three control mixes were manufactured with the same high-quality coarse aggregate (diabase) and three different fines, limestone filler, fly ash and cupola slag powder. All the mixtures were subjected to the same tests, the results demonstrate that steel slag concrete shows an excellent response against carbonation, a slightly lower response against thermal shock cycles, similar drying shrinkage and a superior response against the action of freezing-thawing cycles and abrasion wear in comparison to the control mixes.

1. Introduction

The manufacture of sustainable concrete is one of the main challenges in the field of construction materials. The generation of electric arc furnace slags (EAFS) grew to 18 Mt in Europe in 2016 [1], while part of this amount and other industrial waste continue to end up in landfills. The valorization of steel industry by-products involves not only a reduction in the environmental impact, but also economic and energy savings. Both EAFS, due to its high strength, and cupola slag, due to its pozzolanic activity, are two clear examples of the great potential steel industry by-products have for the manufacture of structural concrete [2].

Cupola slag is a waste generated in the process of obtaining ductile iron in cupola furnaces and that comes mainly from coke ash, from refractory lining fluidized in fusion or from oxidation products of iron and scrap. When the slag undergoes rapid cooling, its vitrification is favored, leaving the silica in an amorphous structure and, thus, susceptible to reacting. The process of valorization of this waste has been discussed by the authors in a previous work [3] and its demonstrated pozzolanic properties [4] make it suitable to be incorporated as supplementary cementing material (SCM). In the case of electric arc furnace slags (EAFS), slow cooling promotes the generation of a stable crystal structure and the chemical inertization of the material. Although compounds such as of free periclase (MgO) and lime (CaO) are highly expansive compounds and can be found in EAFS [5], their content is usually very low and the expansiveness of EAFS is usually very low even before applying treatments of inerting. These stabilization treatments have been widely studied in the literature and are based on hydration (e.g., weathering, water steam treatment or autoclaving) [6].

There is already experience in the manufacture of self-compacting concrete using special aggregates [7], but not using EAFS, to produce high-performance concrete. The first difficulty appears during the concrete mix design, due to a significant lack of fine aggregate, making necessary the incorporation of natural sand and/or filler [8–10]. In this way, to obtain high-performance self-compacting concrete, reactive fillers can be used, where the reaction of the portlandite ($Ca(OH)_2$) released in the hydration of the clinker components with the pozzolans, gives rise to additional hydrated calcium silicate [11]. The use of such admixtures enables the manufacture of high-performance concrete [12] improving compactness as well as flowability, reducing intergranular interaction [13] and increasing cohesion and resistance to segregation [14,15]. On the other hand, the use of the cupola slag as an admixture represents a novel application that has not been exploited. It has been demonstrated that the use of cupola slag as aggregate in concrete is

* Corresponding author.
E-mail address: thomasc@unican.es (C. Thomas).

https://doi.org/10.1016/j.cemconcomp.2021.104399
Received 19 June 2020; Received in revised form 25 November 2021; Accepted 26 December 2021
Available online 2 January 2022

unfeasible [16] as it leads to very poor mechanical properties, but its high content in amorphous silica means it provides high expectations as SCM.

Concrete produced with EAFS aggregates is more eco-efficient [17] and shows a slight increase in density [10,18] and an improved paste-aggregate interface transition zone (ITZ), due to the angularity and roughness of EAFS, which enables better bonding with the cement paste than natural aggregates [19–22]. However, this interaction has a negative impact on the flowability of the concrete, making it necessary to use a large amount of superplasticizer admixture [23]. The high mechanical strength of the EAFS and the improvement of the ITZ usually provides the concrete with a compressive strength increase of up to 50% compared to concrete with natural aggregate, while the high elastic modulus of EAFS also improves frequently the elastic modulus of concrete [24]. On the other hand, there are authors who have obtained losses in terms of strength when incorporating EAFS, so there is some controversy in this regard [25].

Concrete with EAFS has also been shown to have excellent mechanical properties for the production of recycled aggregate concrete (RAC) [26] and its use in multiple recycling stages may be considered [27,28].

The durability of concrete is conditioned by temperature, humidity and fluid transport capacity [29]. The deterioration due to carbonation, as well as the resistance to drying-wetting and freezing-thawing cycles depend, therefore, on the values of capillarity absorption or porosity of the concrete [30,31]. The lack of fine aggregate and the higher EAFS macro-porosity (more cavities) means that the particles have a higher specific surface area and more voids where the paste is housed, so the concrete requires more cement paste to achieve similar structures as a conventional concrete [32]. This means, a priori, that conventional concrete has better durability (as long as the pores are not large) if there is no compensation for fine aggregates. Otherwise, there are studies that suggest a good durability of concretes with EAFS aggregates [25]. In the case of resistance to freezing-thawing cycles the existence of an ordered pore network also enables the dissipation of stresses in the concrete.

Drying shrinkage, on the other hand, is proportional to the volume of the paste [33,34] and also depends on the elastic modulus of the concrete [35]. A self-compacting concrete has a large amount of paste, while concrete with steel aggregates has a high elastic modulus, thus, the deformability effects are opposite.

The durability of concrete against wear abrasion depends largely on the properties of the aggregate [36]. Although the excellent properties of diabase aggregate, commonly used in asphalt concrete [37], are well known, and EAFS shows enough strength and surface hardness to hold high expectations for the concrete manufactured with it to have high resistance to abrasion [38], in fact, there are many recent studies on the use of EAFS either in pervious concrete [39–41] or asphalt concrete [42]. In general, steel slag aggregates have seen much use as abrasion resistant aggregates in asphalt concrete.

The purpose of this study is to demonstrate the high durability of a self-compacting, high-performance concrete using EAFS as aggregate and cupola slag as admixture. There are no studies in the literature on the production of this type of eco-friendly concrete, so there is no characterization of its durability either. In order to achieve this, three control mixes were manufactured, with high quality aggregates (diabase) and different types of fine aggregates (limestone filler, fly ash and cupola slag), to evaluate the feasibility of cupola slag powder as SCM and for comparison with a fourth mix that incorporates EAFS and cupola slag. The mix of these shows an excellent response against gas ingress, a slightly lower resistance to aging by thermal shock, a similar shrinkage and a superior behavior against the action of freezing-thawing cycles and abrasion wear of the control mixes.

2. Materials and methodology

2.1. Materials

The mix design was carried out using diabase coarse 6/12 (DC), diabase sand 0/6 (DS) and silica sand 0/2 (SIS) as natural aggregates. The siderurgical aggregate used was electric arc furnace slag (EAFS) as coarse 6/12 (SC) and fine 0/6 (SLS) aggregates. Three types of additions were also used: limestone filler (LF), fly ash (FA) and cupola slag powder (CS), which were locally available at the time of the study. The aggregate grading was determined according to EN 933-1 and is shown in Fig. 1.

The oxide compositions of the siderurgical by-products used (EAFS and cupola slag) were obtained by Energy-Dispersive X-ray spectroscopy (EDX) and are shown in Table 1. EAFS has a high iron and calcium oxide content, while the cupola slag, which shows an amorphous structure, has high concentrations of amorphous SiO_2 (as shown in a previous research [39], indicator of possible pozzolanic material), calcium and aluminum oxides. In addition, EAFS shows a very low expansivity, close to 0.16% at 24 h and 0.17% at 168 h, according to EN 1744-1 from which it can be deduced that the lime present in the slags is not free lime.

The mix proportions were obtained by means of the methodology proposed by Dinakar et al. [43], based on the compressive strength (100 MPa at 90 days) and the recommendations of the EHE-08 [29] and EFNARC standards [44] for self-compacting concretes. A quantity of 450 kg/m^3 of CEM I 52.5R (EN-197-1), 2% (CEM %wt.) of superplasticizer admixture (SPA) and 550 kg/m^3 of fines (cement + filler or SCM) were used. Three control concrete mixes were manufactured with three different filler materials (limestone, fly ash and cupola slag) using the same volume of admixture in each mix. The fourth mix uses steel aggregate and cupola slag filler, in order to assess the effect of replacing both conventional aggregate and conventional filler. The mix proportions used are shown in Table 2, using analogous proportions for the three control concrete mixes and slightly increasing the fine content in the fourth mix so as to improve workability, reduced by the use of EAFS.

Table 3 shows the characterization of concrete workability as well as hardened state after 28 days under optimal curing conditions, which was reported by the authors in a previous work [32]. The rheology of the concrete mixes was obtained by the slump flow test according to EN 12350-8, the L-box test performed according to EN 12350-10 using 3 bars and the V-funnel test performed according to EN 12350 -9. Regarding the physical properties, the apparent specific gravity (ρ_a) was determined according to EN 12390-7 and the open porosity was determined applying air vacuum according to the UNE 83980 standard. Regarding the mechanical properties, the compressive strength (f_c) was determined following EN 12390-3 and the compressive stabilized elastic modulus (E) following the methodology proposed by EN 12390-13. When using the cupola slag, the mechanical properties are improved, while workability remains practically the same. More tests at different ages were performed in the aforementioned work.

The concrete was mixed in a 120 l rotating drum mixer, in batches of 30 l with a mixing time of 12 min. The specimens were removed from the mold 16–24 h after manufacturing and placed in a moisture chamber,

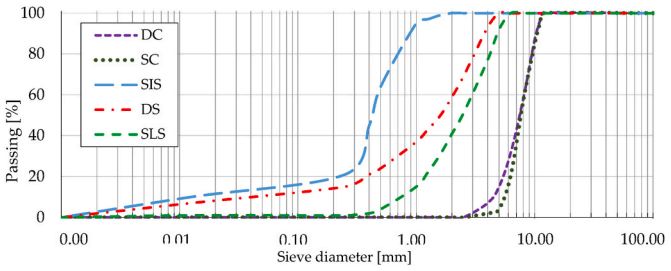

Fig. 1. Aggregate grading curves.

Table 1
Slag Oxide composition.

Compound [wt. %]	Fe_2O_3	CaO	SiO_2	Al_2O_3	MgO	MnO	Cr_2O_3	TiO_2	Others
EAFS	37.90	30.26	12.00	7.40	4.93	4.53	1.15	0.53	<0.5
Cupola slag	6.34	29.97	43.56	13.64	2.10	2.80	–	0.51	<0.5

Table 2
Concrete mixtures (kg/m^3).

Component	SCC-DC-LF	SCC-DC-FA	SCC-DC-CS	SCC-SC-CS
Diabase coarse (DC)	896	896	896	–
EAFS coarse (SC)	–	–	–	1101
Diabase sand (DS)	411	411	411	–
Silica sand (SIS)	386	386	386	605
EAFS sand (SLS)	–	–	–	444
Limestone filler (LF)	100	–	–	–
Fly ash (FA)	–	80	–	–
Cupola slag filler (CS)	–	–	109	109
CEM	450	450	450	450
Water	180	180	180	174
Superplasticizer admixture	9	9	9	9
w/c ratio	0.40	0.40	0.40	0.39

Table 3
Rheological and physical-mechanical properties of concrete at 28 days [32].

Concrete	V Funnel test [s]	L-Box test [%]	Slump flow [mm]	ρ_a [g/cm^3]	Porosity [% Vol.]	f_c [MPa]	E [GPa]
SSC-DC-LF	80	89	755	2.47	5.98	93.3 ± 5.2	41.9 ± 0.3
SSC-DC-FA	46	94	780	2.29	11.59	91.1 ± 2.6	36.9 ± 0.2
SSC-DC-CS	89	96	770	2.48	6.90	104.0 ± 3.7	45.9 ± 0.2
SSC-SC-CS	136	86	690	2.88	5.21	109.5 ± 5.9	56.9 ± 0.4

where they were cured for 28 days at 95 ± 5% relative humidity and 20 ± 2 °C temperature.

After the curing process, the specimens' durability was tested by the study of length changes, behavior against accelerated carbonation, drying-wetting cycles, freezing-thawing cycles and abrasive wear resistance.

2.2. Determination of the length changes

The concrete length change assessment (dimensional stability) was carried out on two prismatic specimens of 50 × 50 × 300 mm in length per mix (8 in total). Measurements started 24 h after demolding and continued up to 130 days of age, according to UNE 83318, keeping the specimens in air.

The longitudinal variation measurement on the specimens was carried out by comparing them to a 300 mm long steel bar using an analog comparator of 0.01 mm resolution. The specimens were always placed in the same orientation in the testing frame. The length change of the specimens (ε_d) was obtained using the initial length (l_0) and the length reported in each daily measurement (l_f) according to the expression:

$$\varepsilon_d[\%] = \frac{100 \times (l_f - l_0)}{l_0} \quad (1)$$

2.3. Accelerated carbonation

For the accelerated carbonation test, standardized cylindrical specimens of 150 × 300 mm were initially cut into three thirds of 100 mm in height. Subsequently each third was cut longitudinally to finally obtain two sub-specimens. Thus, 6 specimens per mix were tested (24 in total) at a rate of 2 specimens per age, obtaining the carbonation depth at 7, 28, and 90 days of exposure after 365 days of curing. The initial CO_2 concentration in the chamber was 30% by volume which came down to 5% every week when the interior of the chamber was ventilated and the air and CO_2 were renewed.

After the exposure time of the specimens, at first a visual inspection was performed to detect signs of surface degradation. Then, each subsample was split in half in the direction of the generatrix in order to spray a solution with 1% by weight phenolphthalein into a solution of 70% ethyl alcohol (96% purity) and 30% distilled water (UNE 112011) on the cracking surface. Finally, the maximum carbonation depth was determined by means of a caliper on the unmarked area.

2.4. Thermal shock aging

The thermal shock aging tests were carried out on three cubic, 50 mm side, specimens per mix (12 in total). Samples were obtained by cutting the prismatic specimens used in the length variation test (50 × 50 × 300 mm), the ends of each prismatic specimen were discarded. Two control cubes per mix of the same dimensions were also used. In the absence of standards, a methodology that consists in subjecting the specimens to 100 drying-wetting cycles was developed.

Each cycle begins with 8 h of immersion in water at 20 ± 2 °C, keeping the water level 20 mm above the specimens. Then, the specimens were placed in an oven for 16 h at 110 ± 5 °C; their mass was measured daily and once a week the ultrasonic pulse velocity (UPV) was obtained. The UPV was determined according to EN 12504-4, placing the transducers opposite each other aligned on the cast surfaces.

Before starting the cycles, specimens were oven dried at 110 ± 5 °C, registering their initial mass and UPV. At the end of the cycles, the compressive strength of both, the control (f_{CC}) and aged specimens (f_{CT}), was determined in accordance with EN 12390-3. Finally, the compressive strength variation was (Δf_C) calculated as:

$$\Delta f_C[\%] = \frac{100 \times (f_{CC} - f_{CT})}{f_{CC}} \quad (2)$$

2.5. Freeze-thaw cycles

Three cubic, 50 mm side, specimens were subjected to freeze-thaw cycles per mix (12 in total) after curing 28 days. The test specimens were obtained as described in the thermal shock aging. The specifications of EN-12390-9 were followed, although the size of the specimens proposed in the standard is higher (100 × 100 mm cubes), and the concentration of NaCl in the solution used (5%) is greater than the (3%) proposed, so the test carried out is much more aggressive than the standardized and equally valid for comparative purposes. The specimens have been placed in a metal container maintaining minimum separation distances, while the temperature control throughout the cycles was determined by placing a thermocouple in the core of one of the test specimens (Fig. 2a).

The cooling cycle lasts 16 h and ends at −20 °C while the heating cycle lasts 8 h and ends at 20 °C. Throughout the cycle, samples were totally immersed in the test solution which was renewed weekly when the detached fragments were removed and specimens were photographed. Only when any specimen was not suitable for the compressive

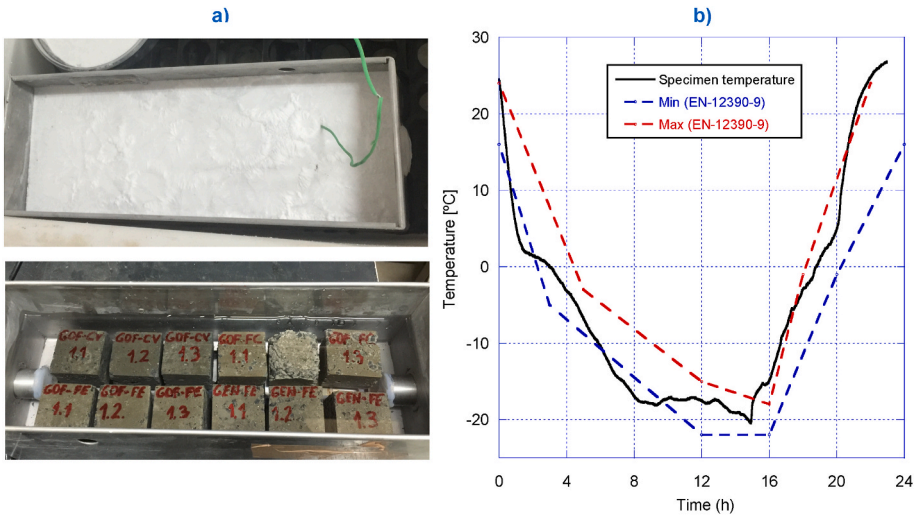

Fig. 2. Experimental setup (a) and temperature registered inside the specimens during freeze-thaw cycle (b).

strength test, due to the loss of its cubic shape, was it considered disintegrated and removed. Fig. 2b shows both, the temperature registered within the specimen during one cycle and the (Min/Max) limits established in standard 12390-9.

2.6. Mechanical durability: abrasive wear resistance

Three cylindrical specimens of 150 × 100 mm were cut as described in the accelerated carbonation test to determine the abrasive wear resistance on 12 subsamples by means of the "the wide disc test" described in the EN 1338 standard, using corundum (white fused alumina) as the abrasive agent with a F80 grain size according to ISO 8486-1 standard.

The test subsamples were dried at 110 ± 5 °C and subsequently sprayed with black paint on the test surfaces to facilitate the measurement of the wear marks.

During the test, the abrasive disc rotates at 75 rpm in contact with the abrasive agent and the surface of the specimen for 1 min. After the test, the mark generated is measured at three points with a caliper, the largest mark is considered the test result.

3. Results and discussion

3.1. Length changes

The concrete length changes are mainly due to external forces, temperature changes, drying shrinkage or aggregate expansivity. Keeping the first two constant, the factors that influence the variation in length are drying shrinkage, produced during cement hydration, and CaO and MgO hydration.

In any case, expansivity was observed due to the valorization process applied on the steel industry slags in order to produce the EAFS. Fig. 3 shows that the average drying shrinkage in no case exceeds 0.025% (250 μm/m), using the same amount of cement in all mixes. The SCC-DC-LF showed the least shrinkage after stabilizing at 60 days, while the greatest change in length corresponded to SCC-DC-FA, the mix with the highest porosity. Concrete porosity is a factor that greatly affects the length variation due to the stiffness decrease as a result of a higher porosity enabling greater deformations when loaded. Compared to the other two mixtures with DC and different SCM, SCC-DC-CS showed 20% higher drying shrinkage than SCC-DC-LF due to a 13% higher porosity and the FA activity. Regarding the mixtures with cupola slag, SCC-DC-CS and SCC-SC-CS, the shrinkage is close to 0.014% in both cases, as would be expected using the same amount of cement and slag powder, despite

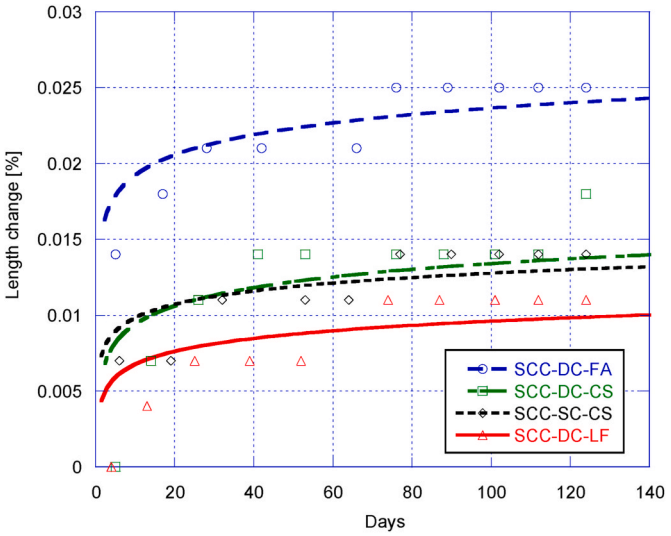

Fig. 3. Drying shrinkage for 130 days.

the higher porosity of the SCC-DC-CS.

In conclusion, mixtures incorporating cupola slag powder showed slightly higher drying shrinkage than the control mix and this was attributable to the use of greater amounts of cementitious and SCM materials (cement + cupola slag).

3.2. Accelerated carbonation

In Fig. 4 it can be observed, by visual inspection, that the material does not show degradation (cracks, detachments or fractures) on its surface after 90 days of exposure. The same figure shows areas where the phenolphthalein solution has been sprayed, showing the surface carbonation of the material.

However, contrasting behavior can be observed inside the test specimens. Phenolphthalein turns red-purple with a pH higher than 9.5 (non-carbonated concrete) and becomes colorless with values lower than 8 (carbonated concrete), taking shades between pink and red-purple for pH values between 8 and 9.5. Fig. 4 shows the mix SCC-SC-CS after 90 days of accelerated carbonation once the phenolphthalein solution had been applied. All the specimens tested showed excellent behavior against accelerated carbonation, 0 mm after 90 days due to their good surface finish, the reduced open porosity (around 6%) and

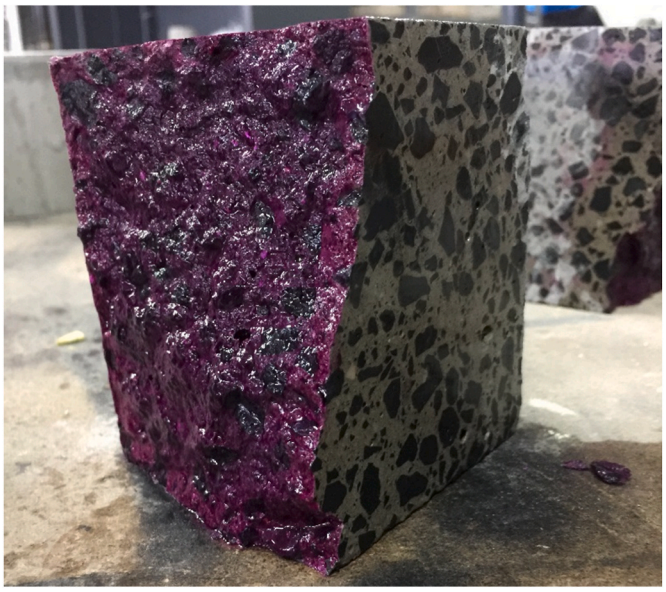

Fig. 4. Appearance of the specimens CO_2-exposed surface after the pH indicator spraying.

packed microstructure of all concretes.

3.3. Thermal shock aging

Fig. 5 shows the dry mass variation after 100 drying-wetting cycles. All specimens underwent a slight increase in mass around of 0.6%. This increase in dry mass is associated with absorption of water during wetting subcycles, which was not able to evaporate during the 16 h of drying. Therefore, for samples in which saturation occurred, a longer drying time was required than that recommended in the regulations in order to reach constant weight.

The mass increase shown in Fig. 5 is higher in SCC-DC-FA and SCC-SC-CS mixes. The first mix has the highest open porosity (Table 3), due to the FA reaction with the SPA, while the second uses EAFS coarse aggregate, whose porosity is 70% greater than the diabase coarse aggregate (two of the exposed sides were cut during the specimen preparation and the aggregate was exposed). The other two mixes with diabase coarse aggregate (SCC-DC-LF and SCC-DC-CS) obtain similar mass gains, so the admixture type does not appear to influence this property. Finally, after complete drying of the specimens, no relevant mass changes were observed.

Fig. 6 shows the UPV decrease of all mixes during the 100 exposure cycles. An optimal fit has been obtained using a negative exponential fit, as well as high R^2 values except in the case of the reference mix, due to a high variability in the results. It can be seen that all the mixes lost UPV in the 4–7% range. This UPV loss is contradictory to the mass gain shown and is due to the internal deterioration of the specimen. On the one hand, although the drying cycle high temperature is not critical, aggregates and paste have different thermal expansion coefficients, even more so when using steel aggregates. On the other hand, the maximum test temperature produces the most volatile products of hydrated paste decomposition such as ettringite (80–150 °C) [45]. The thermal shock cycles result in the appearance of small discontinuities (not visible to the naked eye) that allow a greater volume of water to percolate and decrease the ultrasonic pulse travel time.

The UPV decreases obtained are minimum (good performance) in all the specimens, however, the lowest loss corresponds to the mix with limestone filler (SCC-DC-LF), while the other mixes behave quite similarly and provide the highest UPV decrease.

Table 4 shows the control specimens' compressive strength (initial compressive strength), the residual compressive strength of the specimen subjected to 100 drying-wetting cycles and the relative variation between these the SCC-DC-FA mix varies its relative strength most, suffering losses greater than 10%, induced by its high porosity, which allows a greater water circulation through its internal structure. The SCC-DC-LF mix is not affected in terms of mechanical properties, considering that the initial and residual values fit within the deviations obtained. In the comparison between the SCC-DC-LF and SCC-DC-CS mixes, the best thermal stability is observed in the limestone filler mix, however, the cupola slag powder mix maintains a slightly higher residual compressive strength. The SCC-SC-CS mix suffers a greater loss than the previous two mixes, confirming a greater thermal incompatibility of the siderurgical aggregate with the natural aggregate. However, in absolute terms, this mix has higher residual compressive strength, 15% higher than the limestone-filler control concrete.

Fig. 7 shows the specimens' appearance after 100 cycles. It can be seen that the external deterioration is minimal, being more pronounced on the edges of the cubes. Additionally, on the sides that have been in contact with the mold, some pores that were initially covered by a thin layer of paste have been revealed. In the case of siderurgical aggregate, it

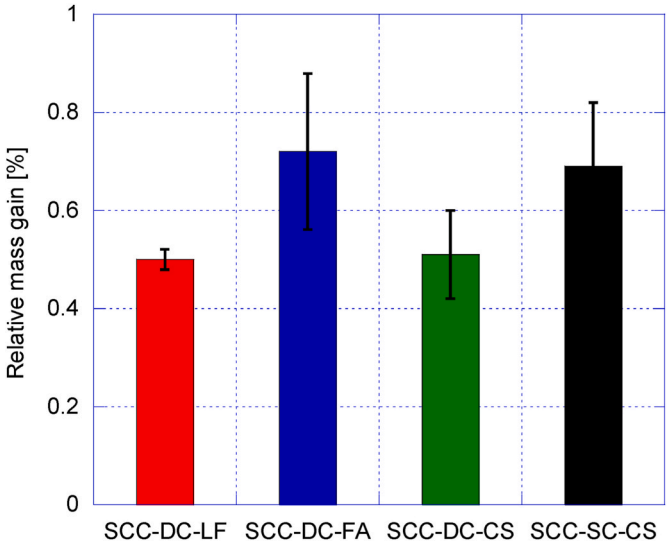

Fig. 5. Relative mass variation after 100 exposure cycles.

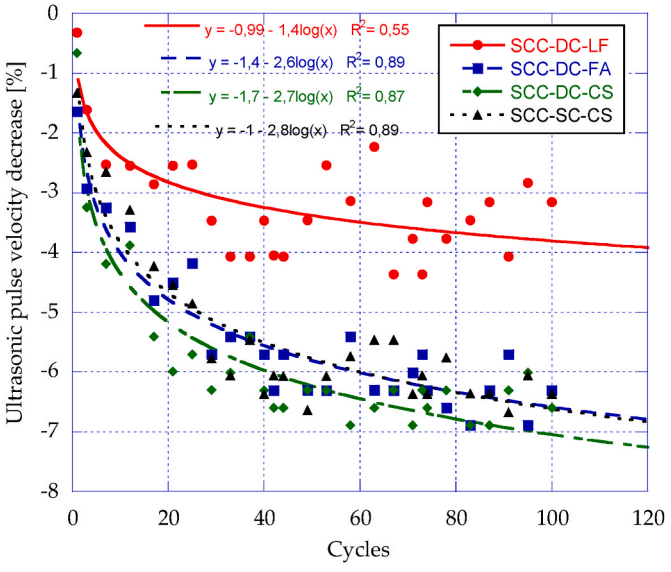

Fig. 6. Ultrasonic pulse velocity variation during 100 thermal shock cycles.

Table 4
Compressive strength variation after the thermal shock cycles.

Mix	Compressive strength [MPa]	Residual compressive strength [MPa]	Relative variation [%]
SCC-DC-LF	100.1 ± 2.3	102.1 ± 3.4	2.0
SCC-DC-FA	101.6 ± 2.5	89.5 ± 4.2	−11.9
SCC-DC-CS	108.6 ± 3.1	102.9 ± 3.6	−5.2
SCC-SC-CS	130.7 ± 1.9	121.5 ± 0.9	−7.0

can be seen that some iron particles present in the slag have been oxidized. This phenomenon only appeared on the cut sides.

3.4. Freezing-thawing cycles

When the water in the concrete pores freezes, it expands, creating stresses. If these stresses exceed the surface paste tensile strength, it starts to peel off. There are conflicting ideas on how to improve freezing-thawing resistance in high-performance concrete (HPC) [46]: reducing its porosity (minimizing the w/c ratio) and thus the freezable water admission or employing air-entraining agents. This latter idea is based on the fact that when entrained air bubbles (with a certain size and spacing) are introduced uniformly into the paste, stresses are cushioned [47].

Table 5 shows the number of cycles that each mix has endured (following the disintegration criterion explained in the methodology) under accelerated aging by freezing-thawing cycles. Due to the high concentration of NaCl in the solution and the small size of the test specimens, the test was especially aggressive in pushing the material to the limit and thus facilitating direct comparison between the different mixes.

The elevated porosity, due to the reaction between the SPA and FA, gives the SCC-DC-FA mix the best performance. On the other hand, the

Table 5
Number of freezing-thawing cycles until disintegration.

	SCC-DC-LF	SCC-DC-FA	SCC-DC-CS	SCC-SC-CS
Cycles	7	>21	11	21

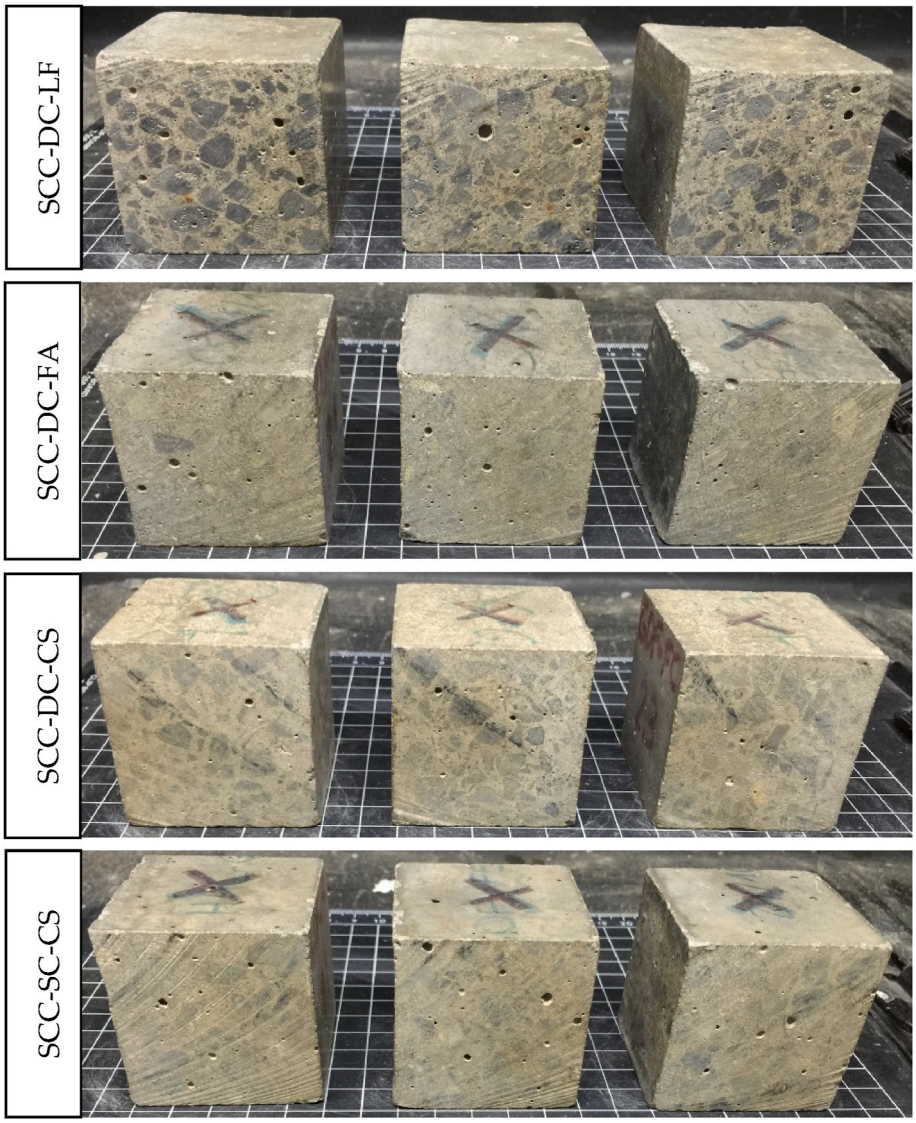

Fig. 7. Test specimen appearance after drying-wetting cycles.

SCC-SC-CS mix tolerated many more cycles than the SCC-DC-LF control mix (3 times more), since it has lowest accessible porosity, and this has prevented the saline solution's entry to a greater extent. The SCC-DC-CS mix has shown an intermediate performance and is clearly superior to the SCC-DC-LF mix, which reflects the better performance of the steel aggregate in freezing-thawing cycles.

Fig. 8 shows the degradation of the specimens after 5 cycles. A good state of conservation is observed in the specimens SCC-DC-FA and SCC-SC-CS, showing the first stages of degradation in the corners and slightly on the edges of the cubes. The SCC-DC-CS mix shows greater degradation on the edges and the material begins to detach from the surface faces. The SCC-DC-LF mix shows more severe degradation with more detachments on the cube sides and at the corners. More advanced deterioration conditions include the specimens "spherification" and subsequent disintegration.

Fig. 9 shows the specimens that incorporate cupola slag powder and the two types of aggregate (SCC-DC-CS and -SCC-SC-CS), after undergoing 7 freezing-thawing cycles. It can be observed that the first stages of degradation occur mainly in the weakest areas like corners, edges and thin mortar layers that cover the aggregates. Then aggregate detachment takes place, increasing the mortar surface and boosting the deterioration process. EAFS is less susceptible due to its greater bonding to the paste.

3.5. Mechanical durability: abrasive wear resistance

The abrasive wear resistance will depend exclusively on the aggregate hardness and the SCM used, since all the concrete mixes use the same type and quantity of cement. Table 6 shows the wear mark widths obtained on each of the cylindrical specimen thirds tested: upper, middle and lower. The wear marks observed in all mixes are similar and small in size, with small differences. In all cases the mark width is less than 20 mm, meeting the requirement for the most demanding class (class 4) according to EN 1338. Mixes with diabase coarse and conventional SCMs (SCC-DC-LF and SCC-DC-FA) show the same wear mark, close to 16 mm, which denotes a similarity between the two SCMs and also that the concrete porosity (90% higher using FA) is not a decisive factor in this property. Additionally, diabase is an excellent aggregate for asphalt concrete due to its high resistance to rolling wear, as well as its mechanical performance [37].

Analyzing the similarity found between the SCC-DC-CS and SCC-SC-CS, it is shown that the wear behavior of both aggregates, diabase and EAFS, is very similar. This likeness is similar to that found in Los Angeles coefficient test following EN 1097-2 (15% for both materials), so there is

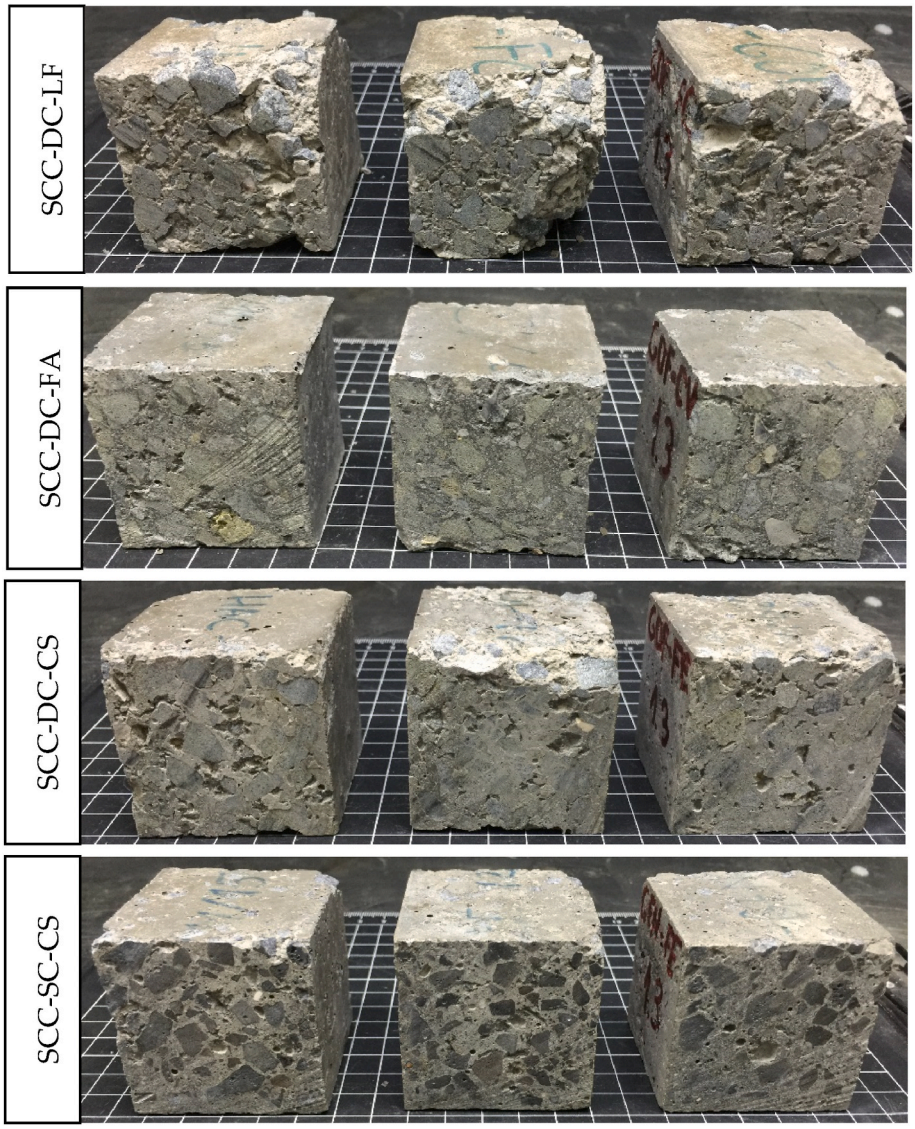

Fig. 8. Test specimen appearance after 5 freezing-thawing cycles.

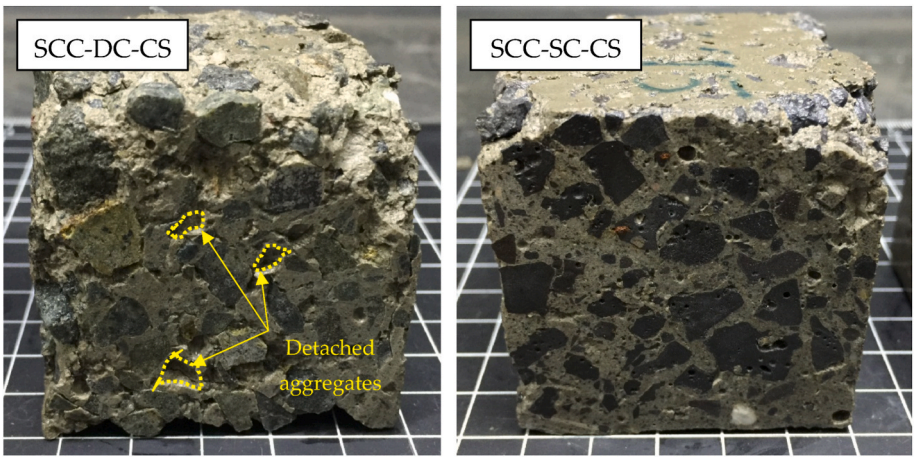

Fig. 9. Cupola slag specimen appearance after 7 freezing-thawing cycles.

Table 6
Abrasion wear marks (mm) on the cylindrical specimen thirds.

Specimen third	SCC-DC-LF	SCC-DC-FA	SCC-DC-CS	SCC-SC-CS
Upper	17.0	17.0	16.0	15.5
Central	16.0	16.0	15.0	15.5
Lower	15.5	16.0	15.0	15.0
Average	16.2 ± 0.76	16.3 ± 0.58	15.3 ± 0.58	15.3 ± 0.29

an obvious relationship between the abrasion resistance of aggregates and the abrasive wear resistance of concrete. On the other hand, the differences found between the use of conventional SCM and cupola slag indicate that the slag provides the paste with greater resistance to abrasion wear.

Analyzing the variation of the behavior on the specimen height, it is observed that the smallest abrasion mark corresponds to the lower third in all cases. This is due to the tendency to a better consolidation at the bottom of the specimen during hardening, although this effect is reduced in the SCC-SC-CS mix despite using a denser aggregate (less segregation). Fig. 10 shows the marks produced by abrasion on the specimens.

4. Conclusions

This research deals with the durability characterization of high-performance self-compacting concrete produced with two siderurgical by-products: EAFS (strength contribution) and cupola slag (pozzolanic contribution). The analysis of results and the comparison with the control mixes that use high-quality aggregates (diabase) and conventional SCM, enable the following concluding remarks to be made.

- Length changes due to drying shrinkage at 130 days are 20% greater in mixes incorporating cupola slag. This increase is due to having a greater amount of cementitious materials (cement + cupola slag).
- All mixes tested offer an excellent response against accelerated carbonation, even at 90 days of exposition. The reduced CO_2 ingress is due to the dense paste microstructure on the specimen's surface, as well as the low open porosity values, around 6% in all cases.
- The UPV decrease after thermal shock cycles is low for all mixes, the limestone filler mix shows the best performance (−3.8% at 100 cycles), while the siderurgical aggregate mix decrease is 70% greater, as well as 9% greater residual compressive strength loss.
- The siderurgical aggregate mix is able to endure three times more freezing-thawing cycles than the limestone filler control mix. However, the fly ash mix shows superior response to the cycles due to the

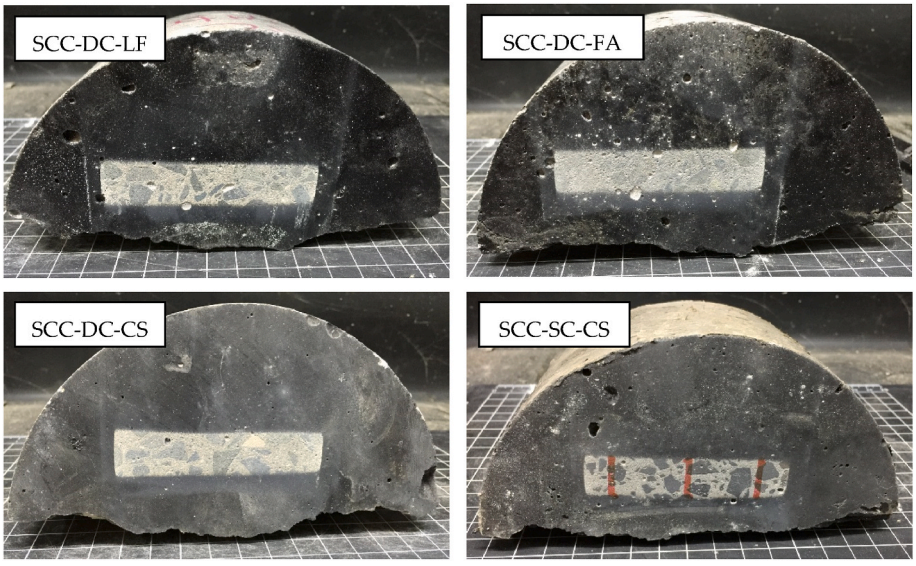

Fig. 10. Abrasion wear test marks.

pore network generated in the reaction with the superplasticizer admixture, which cushions the stresses during the freezing sub-cycles.

- Durability against wear abrasion is excellent using both diabase and steel slag aggregate (slightly higher in the latter), both with high resistance to fragmentation. On the other hand, the determination of the abrasive wear resistance on different specimen heights enables the assessment of the aggregates' wear distribution, with a small increase on the upper thirds.

Declaration of competing interest

The authors declare that they have no known competing financial interests or personal relationships that could have appeared to influence the work reported in this paper.

Acknowledgments

The authors of this research would like to thank the GLOBAL STEEL WIRE plant in Santander (Celsa Group) for the EAF slag supply and the Saint Gobain Pam España plant in Santander (Spain) for the Cupola Furnace Slag as well as ROCACERO for providing the cement and superplasticizer.

References

[1] EUROSLAG, https://www.euroslag.com/research-library-downloads/downloads/. Accessed 19 Feb 2020.
[2] J.M. Manso Villalaín, S. Marquínez, Investigación de nuevos usos de las escorias de horno eléctrico de arco (EAF). La oportunidad de los hormigones, Hormigón y Acero. 57 (2006).
[3] I. Sosa, P. Tamayo, J.A. Sainz-Aja, A. Cimentada, J.A. Polanco, J. Setién, C. Thomas, Viability of cupola slag as an alternative eco-binder and filler in concrete and mortars, Appl. Sci. 11 (2021) 1957.
[4] C. Thomas, J. Sainz-Aja, I. Sosa, J. Setién, J.A. Polanco, A. Cimentada, Physical-mechanical properties of cupola slag cement paste, Appl. Sci. 11 (2021) 7029.
[5] E. Vázquez, M. Barra, Reactividad y expansión de las escorias de acería de horno eléctrico con sus aplicaciones en la construcción, Mater. Construcción 51 (2001) 137.
[6] J.M. Manso, J.A. Polanco, M. Losanez, J.J. Gonzalez, Durability of concrete made with EAF slag as aggregate, Cement Concr. Compos. 28 (2006) 528–534.
[7] F. Fiol, C. Thomas, C. Muñoz, V. Ortega-López, J.M. Manso, The influence of recycled aggregates from precast elements on the mechanical properties of structural self-compacting concrete, Construct. Build. Mater. 182 (2018) 309–323, https://doi.org/10.1016/j.conbuildmat.2018.06.132.
[8] J.M. Manso, J.J. Gonzalez, J.A. Polanco, Electric arc furnace slag in concrete, J. Mater. Civ. Eng. 16 (2004) 639–645, https://doi.org/10.1061/(ASCE)0899-1561 (2004)16:6(639).
[9] J.M. Manso, Fabricación de Hormigón Hidraúlico con escoria negra de Horno Eléctrico de Arco, Doctoral thesis, University of Burgos, 2001.
[10] C. Pellegrino, P. Cavagnis, F. Faleschini, K. Brunelli, Properties of concretes with black/Oxidizing electric arc furnace slag aggregate, Cement Concr. Compos. 37 (2013) 232–240.
[11] A.L.A. Fraay, J.M. Bijen, Y.M. de Haan, The reaction of fly ash in concrete a critical examination, Cement Concr. Res. 19 (1989) 235–246.
[12] A.C.I. committee, 363, Report on High-Strength Concrete, American Concrete Institute, USA, 2010.
[13] M. Uysal, K. Yilmaz, Effect of mineral admixtures on properties of self-compacting concrete, Cement Concr. Compos. 33 (2011) 771–776, https://doi.org/10.1016/j.cemconcomp.2011.04.005.
[14] F. Puertas, H. Santos, M. Palacios, S. Martínez-Ramírez, Polycarboxylate superplasticiser admixtures: effect on hydration, microstructure and rheological behaviour in cement pastes, Adv. Cement Res. 17 (2005) 77–89, https://doi.org/10.1680/adcr.17.2.77.65044.
[15] G. Ye, X. Liu, G. De Schutter, A.-M. Poppe, L. Taerwe, Influence of limestone powder used as filler in SCC on hydration and microstructure of cement pastes, Cement Concr. Compos. 29 (2007) 94–102, https://doi.org/10.1016/j.cemconcomp.2006.09.003.
[16] D. Baricová, A. Pribulová, P. Demeter, Comparison of possibilities the blast furnaceand cupola slag utilization by concrete production, Arch. Foundry Eng. 10 (2010) 15.
[17] J.M.F. de Carvalho, W.C. Fontes, C.F. de Azevedo, G.J. Brigolini, W. Schmidt, R.A. F. Peixoto, Enhancing the eco-efficiency of concrete using engineered recycled mineral admixtures and recycled aggregates, J. Clean. Prod. 257 (2020) 120530.
[18] S. Tomasiello, M. Felitti, EAF slag in self-compacting concretes, Facta Univ. Archit. Civ. Eng. 8 (2010) 13–21.
[19] A.S. Brand, J.R. Roesler, Interfacial transition zone of cement composites with steel furnace slag aggregates, Cement Concr. Compos. 86 (2018) 117–129.
[20] B. Pang, Z. Zhou, X. Cheng, P. Du, H. Xu, ITZ properties of concrete with carbonated steel slag aggregate in salty freeze-thaw environment, Construct. Build. Mater. 114 (2016) 162–171.
[21] W. Yuji, The effect of bond characteristics between steel slag fine aggregate and cement paste on mechanical properties of concrete and mortar, MRS Online Proc. Libr. 114 (1987) 49–54.
[22] C. Thomas, J. Rosales, J.A. Polanco, F. Agrela, 7 - steel slags, in: J. de Brito, F. Agrela (Eds.), New Trends Eco-Efficient Recycl. Concr., Woodhead Publishing, 2019, pp. 169–190.
[23] Y.-N. Sheen, D.-H. Le, T.-H. Sun, Innovative usages of stainless steel slags in developing self-compacting concrete, Construct. Build. Mater. 101 (2015) 268–276.
[24] S. Monosi, M.L. Ruello, D. Sani, Electric arc furnace slag as natural aggregate replacement in concrete production, Cement Concr. Compos. 66 (2016) 66–72.
[25] A.S. Brand, E.O. Fanijo, A review of the influence of steel furnace slag type on the properties of cementitious composites, Appl. Sci. 10 (2020) 8210.
[26] P. Tamayo, J. Pacheco, C. Thomas, J. de Brito, J. Rico, Mechanical and durability properties of concrete with coarse recycled aggregate produced with electric arc furnace slag concrete, Appl. Sci. 10 (2020) 216.
[27] C. Thomas, J. de Brito, A. Cimentada, J.A. Sainz-Aja, Macro-and micro-properties of multi-recycled aggregate concrete, J. Clean. Prod. 245 (2020) 118843.
[28] C. Thomas, J. de Brito, V. Gil, J.A. Sainz-Aja, A. Cimentada, Multiple recycled aggregate properties analysed by X-ray microtomography, Construct. Build. Mater. 166 (2018), https://doi.org/10.1016/j.conbuildmat.2018.01.130.
[29] M. de Fomento de España, Instrucción de Hormigón Estructural (EHE-08), 2008.
[30] S. Assié, G. Escadeillas, V. Waller, Estimates of self-compacting concrete "potential" durability, Construct. Build. Mater. 21 (2007) 1909–1917, https://doi.org/10.1016/j.conbuildmat.2006.06.034.
[31] C. Thomas, J. Setién, J.A. Polanco, J. de Brito, F. Fiol, Micro- and macro-porosity of dry- and saturated-state recycled aggregate concrete, J. Clean. Prod. 211 (2019) 932–940, https://doi.org/10.1016/j.jclepro.2018.11.243.
[32] I. Sosa, C. Thomas, J.A. Polanco, J. Setién, P. Tamayo, High performance self-compacting concrete with electric arc furnace slag aggregate and cupola slag powder, Appl. Sci. 10 (2020) 773.
[33] E. Rozière, S. Granger, P. Turcry, A. Loukili, Influence of paste volume on shrinkage cracking and fracture properties of self-compacting concrete, Cement Concr. Compos. 29 (2007) 626–636, https://doi.org/10.1016/j.cemconcomp.2007.03.010.
[34] R. Loser, A. Leemann, Shrinkage and restrained shrinkage cracking of self-compacting concrete compared to conventionally vibrated concrete, Mater. Struct. 42 (2009) 71–82, https://doi.org/10.1617/s11527-008-9367-9.
[35] P.K. Mehta, P.J.M. Monteiro, Concrete: Microstructure, Properties and Materials, McGraw Hill, 2017.
[36] A. García, D. Castro-Fresno, J.A. Polanco, C. Thomas, Abrasive wear evolution in concrete pavements, Road Mater. Pavement Des. 13 (2012) 534–548.
[37] E. Manthos, Stiffness of asphalt concrete mixture with limestone and diabase aggregates, in: Int. Conf. Bitum. Mix. Pavements, 5th, 2011. Thessaloniki, Greece, 2011.
[38] A. Abdelbary, A.R. Mohamed, Investigating abrasion resistance of interlocking blocks incorporating steel slag aggregate, ACI Mater. J. 115 (2018) 47–54.
[39] W. Shen, Y. Liu, M. Wu, D. Zhang, X. Du, D. Zhao, G. Xu, B. Zhang, X. Xiong, Ecological carbonated steel slag pervious concrete prepared as a key material of sponge city, J. Clean. Prod. 256 (2020) 120244.
[40] X. Chen, G. Wang, Q. Dong, X. Zhao, Y. Wang, Microscopic characterizations of pervious concrete using recycled Steel Slag Aggregate, J. Clean. Prod. (2020) 120149.
[41] G. Wang, X. Chen, Q. Dong, J. Yuan, Q. Hong, Mechanical performance study of pervious concrete using steel slag aggregate through laboratory tests and numerical simulation, J. Clean. Prod. (2020) 121208.
[42] W. Jiao, A. Sha, Z. Liu, W. Jiang, L. Hu, X. Li, Utilization of steel slags to produce thermal conductive asphalt concretes for snow melting pavements, J. Clean. Prod. (2020) 121197.
[43] P. Dinakar, K.P. Sethy, U.C. Sahoo, Design of self-compacting concrete with ground granulated blast furnace slag, Mater. Des. 43 (2013) 161–169.
[44] BIMB, E.R.M.C.O. CEMBUREAU, EFCA, EFNARC, The European Guidelines for Self-Compacting Concrete. Specification, Production and Use, 2005.
[45] I. Hager, Behaviour of cement concrete at high temperature, Bull. Pol. Acad. Sci. Tech. Sci. 61 (2013) 145–154.
[46] M.T. Bassuoni, M.L. Nehdi, The case for air-entrainment in high-performance concrete, Proc. Inst. Civ. Eng. Build. 158 (2005) 311–319.
[47] H. Shang, W. Cao, B. Wang, Effect of fast freeze-thaw cycles on mechanical properties of ordinary-air-entrained concrete, Sci. World J. 2014 (2014).